Journal of
Medicinal Chemistry

Drug Annotation

Discovery of Evobrutinib: An Oral, Potent and Highly Selective, Covalent Bruton's Tyrosine Kinase (BTK) Inhibitor for the Treatment of Immunological Diseases

Richard Caldwell, Hui Qiu, Ben C Askew, Andrew T Bender, Nadia Brugger, Montserrat Camps, Mohanraj Dhanabal, Vikram Dutt, Thomas Eichhorn, Anna S Gardberg, Andreas Goutopoulos, Roland Grenningloh, Jared Head, Brian Healey, Brian L Hodous, Bayard R Huck, Theresa L Johnson, Christopher Jones, Reinaldo C Jones, Igor Mochalkin, Federica Morandi, Ngan Nguyen, Michael Meyring, Justin R Potnick, Dusica Cvetinovic Santos, Ralf Schmidt, Brian Sherer, Adam Shutes, Klaus Urbahns, Ariele Viacava Follis, Ansgar A Wegener, Simone C. Zimmerli, and Lesley Liu-Bujalski

J. Med. Chem., **Just Accepted Manuscript** • DOI: 10.1021/acs.jmedchem.9b00794 • Publication Date (Web): 01 Aug 2019

Just Accepted

is published by the American Chemical Society. 1155 Sixteenth Street N.W., Washington, DC 20036

Discovery of Evobrutinib: An Oral, Potent and Highly Selective, Covalent Bruton's Tyrosine Kinase (BTK) Inhibitor for the Treatment of Immunological Diseases

Richard D. Caldwell,* Hui Qiu,* Ben C. Askew,† Andrew T. Bender, Nadia Brugger, Montserrat Camps,‡ Mohanraj Dhanabal, Vikram Dutt, Thomas Eichhorn, Anna S. Gardberg,§ Andreas Goutopoulos, Roland Grenningloh, Jared Head, Brian Healey,¶ Brian L. Hodous,‖ Bayard R. Huck, Theresa L. Johnson, Christopher Jones, Reinaldo C. Jones, Igor Mochalkin,†† Federica Morandi,‡‡ Ngan Nguyen,§§ Michael Meyring,¶¶ Justin R. Potnick, Dusica Cvetinovic Santos, Ralf Schmidt, Brian Sherer, Adam Shutes,‖‖ Klaus Urbahns, Ariele Viacava Follis, Ansgar A. Wegener, Simone C. Zimmerli, and Lesley Liu-Bujalski

ADDRESS: EMD Serono Research & Development Institute, Inc., 45 A Middlesex Turnpike, Billerica, MA 01821, USA (a business of Merck KGaA, Darmstadt, Germany).

KEYWORDS: BTK, covalent, selective, evobrutinib, kinase

ABSTRACT: Bruton's tyrosine kinase (BTK) inhibitors such as ibrutinib hold a prominent role in the treatment of B cell malignancies. However, further refinement is needed to this class of agents, particularly in terms of adverse events (potentially driven by kinase promiscuity) which preclude their evaluation in non-oncology indications. Here, we report the discovery and preclinical characterization of evobrutinib, a potent, obligate covalent inhibitor with high kinase selectivity. Evobrutinib displayed sufficient preclinical pharmacokinetic and pharmacodynamic characteristics which allowed for in vivo evaluation in efficacy models. Moreover, the high selectivity of evobrutinib for BTK over epidermal growth factor receptor and other Tec family kinases suggested a low potential for off-target related adverse effects. Clinical investigation of evobrutinib is ongoing in several autoimmune diseases, including multiple sclerosis, rheumatoid arthritis, and systemic lupus erythematosus.

INTRODUCTION

Bruton's tyrosine kinase (BTK) is a member of the Tec family of tyrosine kinases, and is expressed in B cells, macrophages, and monocytes, but not in T cells.[1] BTK plays a

crucial role in signaling through the B cell receptor (BCR) and the Fcγ receptor (FcγR) in B cells and myeloid cells, respectively.[2] Indeed, mutations in the human *Btk* gene can result in the B cell specific immunodeficiency, X-linked agammaglobulinemia, which is characterized by a block in pre-B cell differentiation; this leads to a lack of B cells and plasma cells, and markedly reduced levels of serum immunoglobulins.[3] Likewise, *Btk* mutations in mice with X-linked immunodeficiency, and targeted deletion of *Btk* in knockout mice result in defects in B cell development and proliferation.[3,4] However, pharmacological inhibition of BTK has not resulted in depletion of B cells in preclinical models.[5] Consequently, BTK is considered a promising therapeutic target for the treatment of various diseases involving B cell and/or macrophage activation, such as B cell malignancies, asthma, rheumatoid arthritis, systemic lupus erythematosus, and multiple sclerosis.[6,7]

The small molecule irreversible BTK inhibitor, ibrutinib, which covalently targets Cys481 within the ATP-binding pocket, is approved for the treatment of mantle cell lymphoma (MCL), chronic lymphocytic leukemia (CLL)/small lymphocytic lymphoma,

Waldenström's macroglobulinemia, and marginal zone lymphoma, as well as graft versus host disease.[8] Ibrutinib demonstrated clinical efficacy in previously difficult-to-treat lymphomas such as treatment-resistant/refractory CLL.[8,9] However, this first in class BTK inhibitor has also shown side effects, including bleeding, rash, diarrhea, and atrial fibrillation, which have been attributed, in part, to off-target kinase-inhibitory related effects on the epidermal growth factor receptor (EGFR) and other Tec family kinases.[10-13]

With the aim of improving the overall tolerability of BTK inhibitors while maintaining the efficacy of ibrutinib, new BTK inhibitors are being developed that have more refined pharmacologic profiles.[13] Additionally, these agents are designed to circumvent the inhibitory effect of ibrutinib on antibody-dependent cell-mediated cytotoxicity, which may be important for the activity of other oncology therapies administered concomitantly with a BTK inhibitor.[13] In 2017, acalabrutinib became the initial second-generation, covalent BTK inhibitor to be approved by the FDA, for the treatment of MCL.[9,14] However, for chronic autoimmune indications, clinical

development progress has lagged behind that of oncology indications. Recently, there has been increased interest in the development of BTK inhibitors in the autoimmune/inflammatory arena.

Herein, we describe work which led to the identification of the potent and irreversibly covalent BTK[15] inhibitor, evobrutinib (**A18**, M2951) for the treatment of autoimmune diseases. Evobrutinib has excellent kinome selectivity, particularly against EGFR, an acceptable preclinical pharmacokinetic/pharmacodynamic (PK/PD) profile, and is efficacious in in vivo efficacy models of rheumatoid arthritis. Evobrutinib is being evaluated in clinical development for treatment of various immunological diseases.[16]

RESULTS AND DISCUSSION

Medicinal Chemistry Strategy

The target profile for a development candidate for chronic administration in autoimmune diseases included potency, high BTK kinase-selectivity, particularly against EGFR, and moderate clearance. It was hypothesized this profile would result in a low daily dose

which should minimize the risk of liver damage; as covalent binding, combined with a high daily dose, has been reported to be linked to drug-induced liver injury.[17]

To achieve BTK potency and kinase selectivity simultaneously, we employed multiple strategies. First it was desired to have an obligate type covalent inhibitor, in which the covalent binding is essential for the potency of the molecule. Additionally, targeting Cys481 with a warhead to form a covalent bond enhances selectivity because only 10 other kinases: BLK, BMX, EGFR, ERBB2, ERBB4, ITK, JAK3, TEC, MKK7, and TXK contain cysteine in the same region of the receptor. Finally, interaction with the gatekeeper Thr474 further increases selectivity as only 20% of all human kinases have threonine as a gatekeeper residue.[18,19]

Identification of a Novel Hinge Binder

Work to identify suitable chemical starting points began with analysis of the X-ray crystal structure of **B43** (Figure 1, PDB code: 3gen).[18,20] **B43** is a moderately potent inhibitor of BTK and occupies the ATP binding pocket of the BTK kinase domain. The amino-pyrimidine group, acting as a hinge binder, forms interactions with the gatekeeper

residue Thr474, as well as backbone carbonyl and amide N interactions with Glu475 and Met477, respectively. The *O*-linked phenoxy phenyl group occupies the long and narrow selectivity pocket adjacent to gatekeeper Thr474, and the lipophilic cyclopentyl group sits in the ribose pocket, which is near Cys481, providing an indication of the proper vectors and angles for the desired covalent connection.

Figure 1. X-ray Structure of BTK Ligand **B43** Bound to the BTK Kinase Domain.

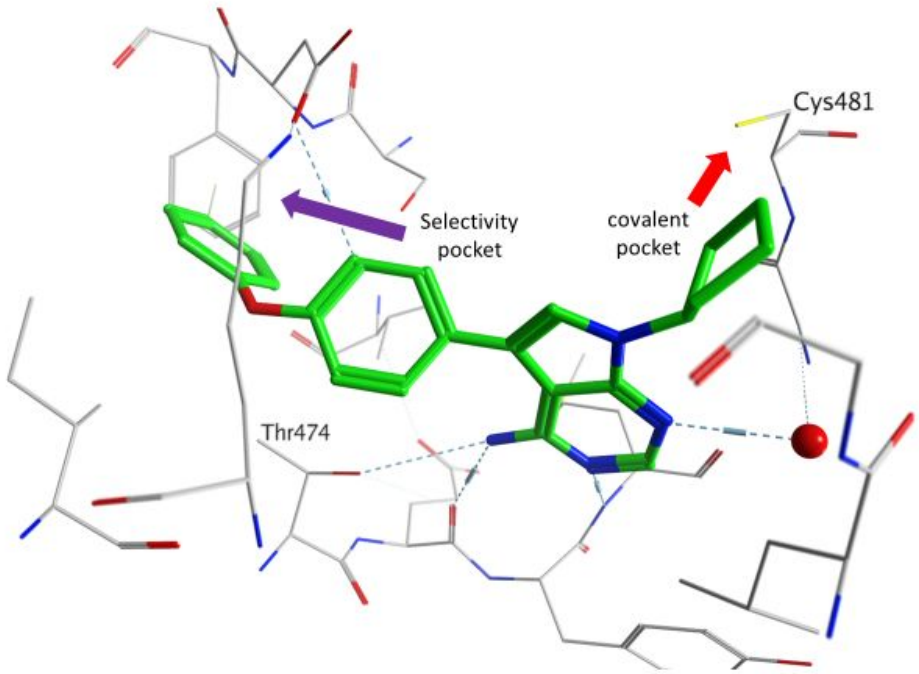

Structure–activity relationship (SAR) exploration focused on replacing the pyrrolopyrimidine of **B43** with other similarly substituted hinge binding moieties bearing aryl linkers appended with an acrylamide warhead. This work revealed that several hinge binding moieties were tolerated for potent BTK inhibitory activity (Table 1). The pyrimidine analog **A3** showed excellent inhibition of BTK in a biochemical assay,[21] while the removal of the 2-amino moiety led to nearly 10-fold loss in potency in compound **A4**. Pyridine analog **A5** also showed excellent BTK inhibitory activity, and both **A3** and **A5** showed 25- to 30-fold more potent inhibition of BTK versus EGFR. However, **A5** had unacceptable activity in the hERG (human ether-a-go-go-related gene) channel assay (Supporting Information). In contrast to **A3** and **A5,** pyrimidine analogs such as **A7**, with opposite orientation of the hinge binder, did not provide an acceptable ratio of inhibition of BTK over EGFR and were subsequently deprioritized. In addition, analysis of the crystal structures of **A5** and **A7** demonstrated that these hinge binders both achieve interactions in the identified hinge region while maintaining the critical vectors and angles required to effectively engage the back pocket and Cys481 as covalent BTK inhibitors (Figure 2). Finally, attaching the linker to the hinge binder through an N atom as in compound **A8** also provided good inhibition of BTK but was equipotent at inhibiting EGFR. Based on these data, the

amino-pyrimidine hinge binder with the amino moiety oriented adjacent to gatekeeper residue Thr474, as in A3 and A5, was selected for further exploration.

Table 1. SAR for Hinge-Binder Optimization

A = 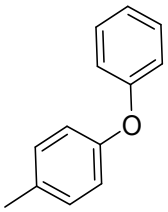

B = 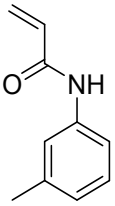

Compound	Hinge-binder group	BTK enzymatic IC_{50} (nM)	EGFR IC_{50} (nM)	hERG % inhibition at 10 μM
B43	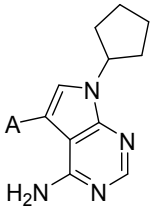	310	177	--
A3	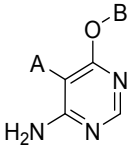	3	78	3%
A4	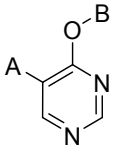	23	--	46%

A5	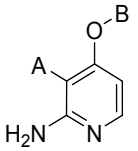	5	140	81%
A6	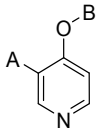	44	--	--
A7	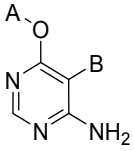	8	1	--
A8	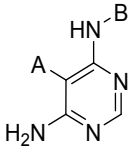	4	4	--

hERG, human ether-a-go-go-related gene; IC_{50}, half maximal inhibitory concentration; Ki, inhibitory constant; SAR, structure–activity relationship

Figure 2. Overlay of Crystal Structures of **A5** and **A7**

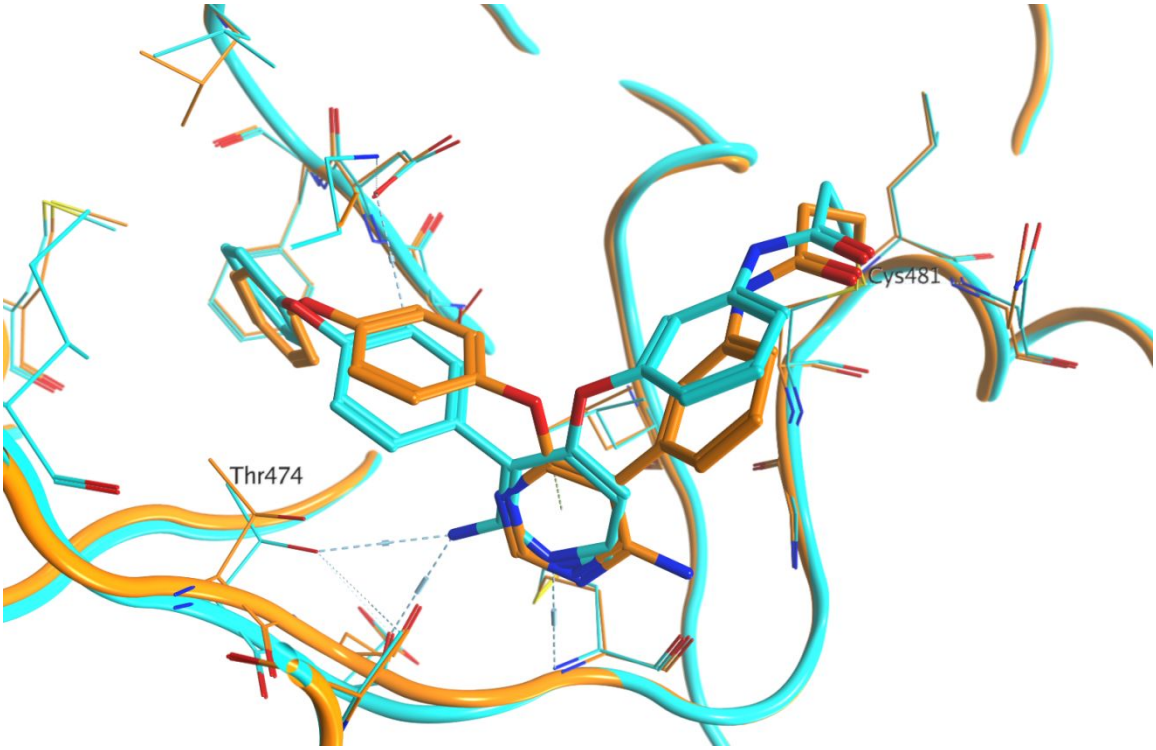

Optimization of the Linker

Further characterization of the hit molecule **A3** showed that, although it demonstrated good potency in the human peripheral blood mononuclear cell (PBMC) assay[21] (IC_{50} = 9.9 nM), this molecule had poor solubility (< 2.4 μM) (Table 2), and poor metabolic stability (high intrinsic clearance, Cl_{int}=277 μL/min/mg) in human liver microsomes. Subsequent efforts focused on modification of **A3** to improve solubility and metabolic stability. Preliminary SAR and X-ray co-crystal information suggested that the

modification of the linker moiety might be amenable for addressing low solubility of the series. Replacing the flat aromatic ring in compound **A3** with a saturated moiety, such as the di-amino cyclohexane ring in analog **A9**, showed good improvement in solubility versus **A3** (134 μM vs 2.4 μM) and metabolic stability (Cl_{int}=27 vs 277 μL/min/mg), without significant loss in enzyme potency.

Various saturated linkers were evaluated with the goal of improving potency in the enzymatic assay (<10 nM). Modifications such as moving the amino group around the cyclohexyl ring, changing the size of the ring, or adding a bridge unit into the linker, maintained the high solubility, however, did not lead to any meaningful boost in potency for **A10**–**A12**. Continued exploration of the linker moiety showed that attachment of the linker to the hinge binding core via a secondary amine, such as in compound **A13**, was not tolerated. It was hypothesized that this substitution caused steric collision between the linker and the protons at the proximal phenyl ring which altered the vector of the linker towards the Cys481. In contrast, analog **A14**, with the reversed linker, was 220-fold more potent in enzymatic assay, but suffered from a poor human microsomal

stability. Additional exploration revealed that the pyrrolidine linker in **A15** was less well tolerated. Introduction of a spiral linker boosted the potency in molecule **A16**. Unfortunately, **A16** showed poor microsomal stability and an unacceptable hERG profile.

Shifting the N atom in **A14** as depicted in **A17** led to a more than 200-fold reduction in enzymatic potency (IC_{50} 1510 nM for **A17** vs 6.5 nM for **A14**). Insertion of one methylene group into **A17** led to the discovery of **A18** (evobrutinib). Evobrutinib **A18** showed excellent potency in the biochemical and PBMC assays, favorable permeability in the Caco-2 assay, good solubility and microsomal stability, and acceptable hERG inhibition (see Supporting Information for assay methods). Finally, a hydroxyl group was added in molecule **A19** to reduce lipophilicity.

Table 2. SAR for Linker Optimization

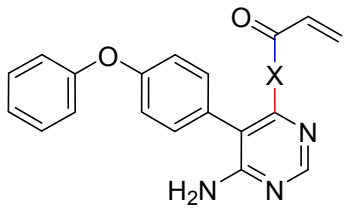

Compound	X (linker) group	BTK enzymatic/PBMC IC_{50} (nM)	Caco-2 P_{app} (A-B) ($\times 10^{-6}$ cm/s)	Caco-2 Efflux ratio	Kinetic solubility (μM)	hERG K_i (nM) or % inhibition at 10 μM	HLM Cl_{int} (μL/min/mg prot.)
A3		2.9/9.9	1.6	4.3	<2.4	3%	277
A8		4.0/19	4.2	1.6	16	530	43
A9	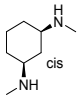	14/--	11.9	3.4	134	1800	27
A10	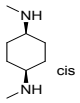	33/660	10	3.7	154	--	41
A11		21/--	23.6	1.5	158	--	202
A12		9.9/70	21.7	1.4	110	1300	36
A13	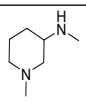	1500/--	--	--	--	--	--
A14		6.5/143	--	--	--	43%	598
A15		5.5/217	25.2	1.0	160	40%	77
A16	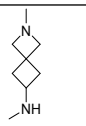	2.1/66	9.3	2.1	153	780	777

A17	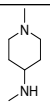	1510/--	--	--	--	--	--
A18	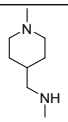	8.9/61	22	1.2	60	3100	110
A19	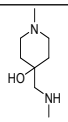	5.9/26	9	3.7	169	45%	68

Cl_{int}, intrinsic clearance; HLM, human liver microsomes; PBMC, peripheral blood mononuclear cell

Back Pocket Optimization

Additional modifications directed to the back pocket to further improve microsomal stability of **A18** (evobrutinib) proved to be unsuccessful (Table 3). Substitutions at the proximal phenyl ring (**A20, A21**) resulted in a dramatic loss in potency on BTK inhibitory activity. No improvement in metabolic stability was observed from modifications of the distal phenyl ring (**A22-A25**). Only analogs **A23** and **A24** displayed similar BTK inhibition compared to **A18**, both with no obvious improvement in clearance. Subsequently, efforts to optimize the back pocket were not pursued further.

Table 3. SAR for Selectivity-Pocket Optimization (Proximal and Distal Ring Modifications)

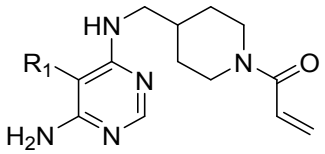

Compound	R_1 group (selectivity pocket)	BTK enzymatic IC_{50} (nM)	HLM Cl_{int} (μL/min/mg)
A18 evobrutinib	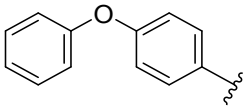	8.9	110
A20	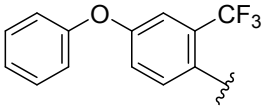	>100,000	--
A21	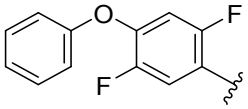	160	143
A22	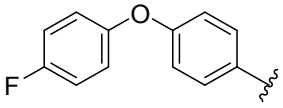	150	143
A23	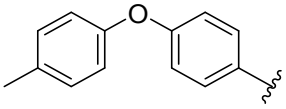	18	145
A24	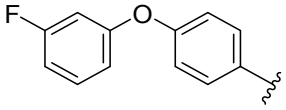	9.0	199
A25	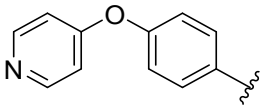	730	688

A26	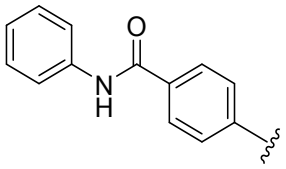	1200	--

BTK, Bruton's tyrosine kinase; Cl_{int}, intrinsic clearance; HLM, human liver microsomes; IC_{50}, half maximal inhibitory concentration.

Warhead Optimization

Identification of an optimal warhead to engage the Cys481 residue was driven by the goal of designing an obligate covalent inhibitor of BTK. A diverse array of warheads was evaluated to optimize potency, reactivity and plasma stability, and to identify a suitable covalent inhibitor for further in vivo studies (Table 4). Analogs bearing an acrylamide warhead such as that of ibrutinib[19] displayed acceptable biochemical and cellular potency, as exemplified in analog **A18**. Replacement of the acrylamide of **A18** by the acetamide moiety in compound **A27** resulted in an analog with no significant BTK inhibitory activity, demonstrating the requirement of a warhead for efficient inhibition of BTK. Compounds such as **A28** – **A30**, bearing warheads that are theoretically highly reactive[22,23] did show excellent enzyme inhibitory activity, but suffered from unacceptable plasma stability. These results were attributed to the high reactivity of the

warheads. It was speculated that these compounds were binding non-specifically to cellular components before they were able to reach the target. Substitution with Michael acceptors that are theoretically less reactive than acrylamide[22,23] led to a decrease in BTK inhibitory activity compared to compound **A18**, as seen with analog **A32**. Based on these data, compound **A18**, bearing an acrylamide warhead, possessed the optimal combination of potency, reactivity, and plasma stability to be selected for additional profiling.

The obligatory nature of covalent inhibition with **A18** was further confirmed by comparing its activity with that of **A27** against a mutant BTK kinase domain with a cysteine to serine substitution, which resulted in a lack of covalent binding by either molecule. Both compounds inhibited the BTK mutant with similarly low potency (IC_{50} 8.6–8.7 μM), reflecting their reversible affinities for the BTK kinase domain without any covalent binding. Thus, while **A27** showed minimal inhibitory activity regardless of Cys481 binding, the approximately 1,000-fold increase in potency of **A18** against the wildtype BTK kinase domain demonstrated that its potency is derived from covalent

engagement of Cys481. Both **A18** and **A19** were further characterized in PK/PD studies in mice.

Table 4. SAR for Warhead Optimization

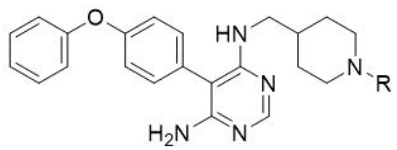

Compound	R_1 group	BTK enzymatic/PBMC IC_{50} (nM)	$K_{irrev} = K_{inac}/Ki$ (1/Ms)	% remaining in plasma at 4 h
A18 evobrutinib	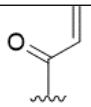	8.9/61	63,000	81
A27		>10000/--	--	--
A28	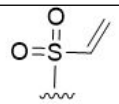	0.8/45	113,000	16
A29	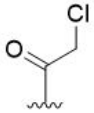	0.6/160	--	49

A30	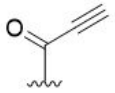	0.2/--	--	34
A31	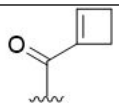	290	--	--

PK/PD Studies

To confirm whether the *in vitro* effects with **A18** and **A19** translated into B cell inhibition in vivo, these compounds were tested head-to-head in a B cell stimulation assay in normal C57BL/6 mice.[24] Both compounds were dosed at 1 mg/kg orally.

Compound **A19** inhibited B cell activation by 42% and 15% at 1 and 24 h after dosing, respectively (Figure 3). Compound **A18** (evobrutinib) achieved a greater B cell inhibition of 71% and 25% at 1 and 24 h. This was despite a lower maximum plasma concentration (C_{max}) of **A18** compared to **A19** (52 nM versus 257 nM). These data showed that **A18** was a more potent B cell inhibitor than **A19** in vivo.

Figure 3. PK/PD Studies in Mice

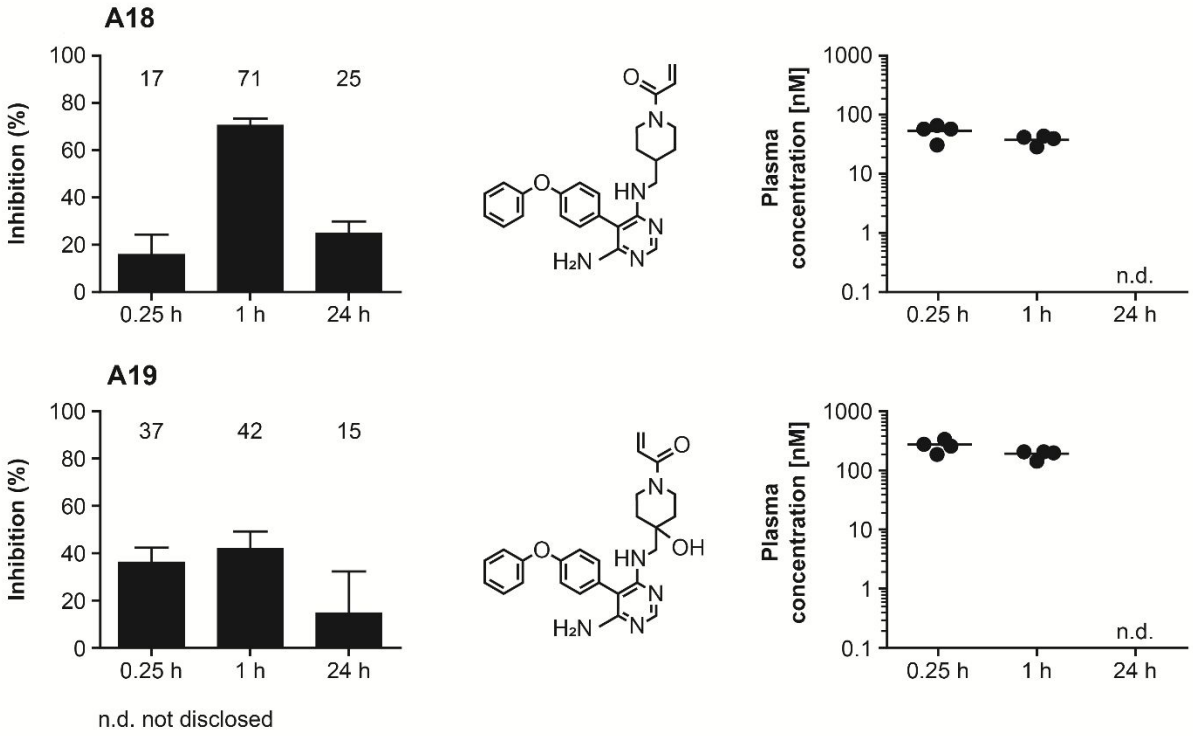

Synthesis of Evobrutinib (A18)

The synthesis of evobrutinib (**A18**) began with regioselective nucleophilic substitution of the 6-chloride of 5,6-dichloropyrimidin-4-amine by the primary amine of *tert*-butyl 4-(aminomethyl)piperidine-1-carboxylate, which led to generation of *tert*-butyl 4-{[(6-amino-5-chloropyrimidin-4-yl)amino]methyl}piperidine-1-carboxylate (Figure 4). Subsequent Suzuki coupling of this chloropyrimidine intermediate with phenoxyphenylboronic acid

yielded the molecule *tert*-butyl 4-({[6-amino-5-(4-phenoxyphenyl)pyrimidin-4-yl]amino}methyl)piperidine-1-carboxylate. Deprotection under acidic conditions and subsequent neutralization afforded the piperidine derivative 5-(4-Phenoxy-phenyl)-*N*-piperidin-4-ylmethyl-pyrimidine-4,6-diamine. Finally, the acrylamide was introduced to give the target compound *N*-[(1-acryloylpiperidin-4-yl)methyl]-5-(4-phenoxyphenyl)pyrimidine-4,6-diamine (**A18**; evobrutinib; step d).

Figure 4. Synthetic Route for Evobrutinib[a]

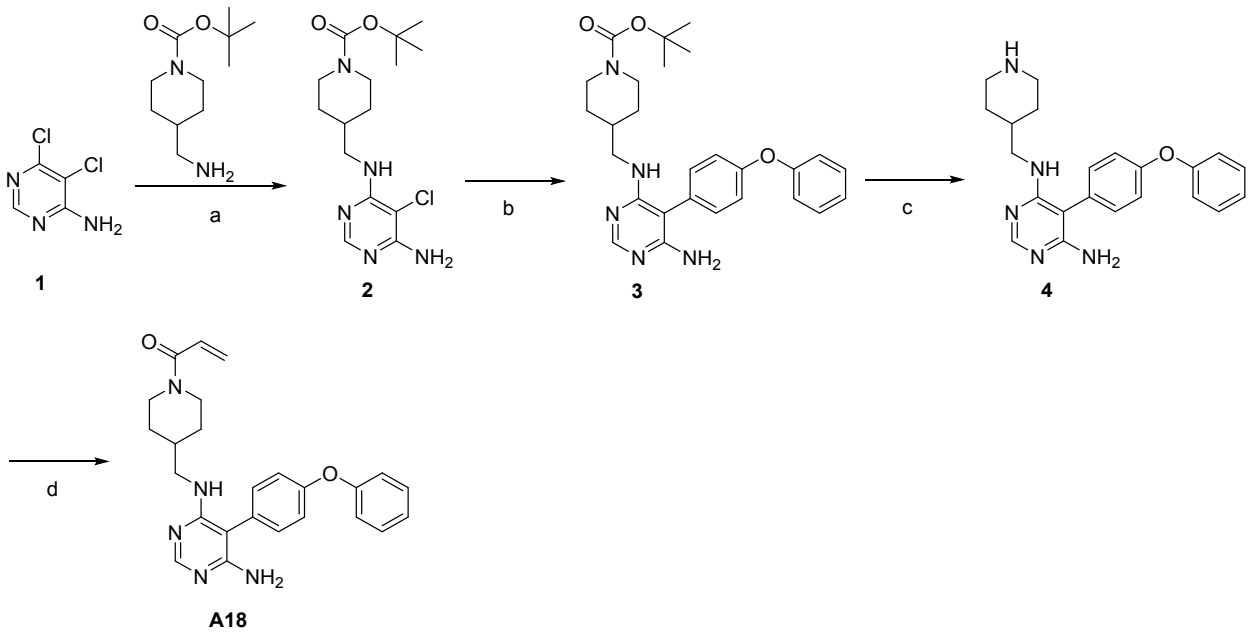

[a](a) DBU, DMF, 90 °C, 91%; (b) 4-phenoxylphenyl boronic acid, $Pd(OAc)_2$, *S*-phos, K_2CO_3, dioxane-H_2O (10:1 v/v), 150 °C, 48%; (c) HCl, MeOH, rt; (d) acryloyl chloride, $NaHCO_3$, H_2O-THF (1:10, v/v), rt, 9%

Characterization of Evobrutinib: Biophysical Confirmation of Covalent, Irreversible Binding

Covalent binding to Cys481 is confirmed by analysis of the X-ray crystal structure of evobrutinib bound to the BTK kinase domain, showing continuous electron density between Cys481 and the evobrutinib warhead (Figure 5).

Figure 5. Crystal Structure of Evobrutinib Bound to the BTK Kinase Domain

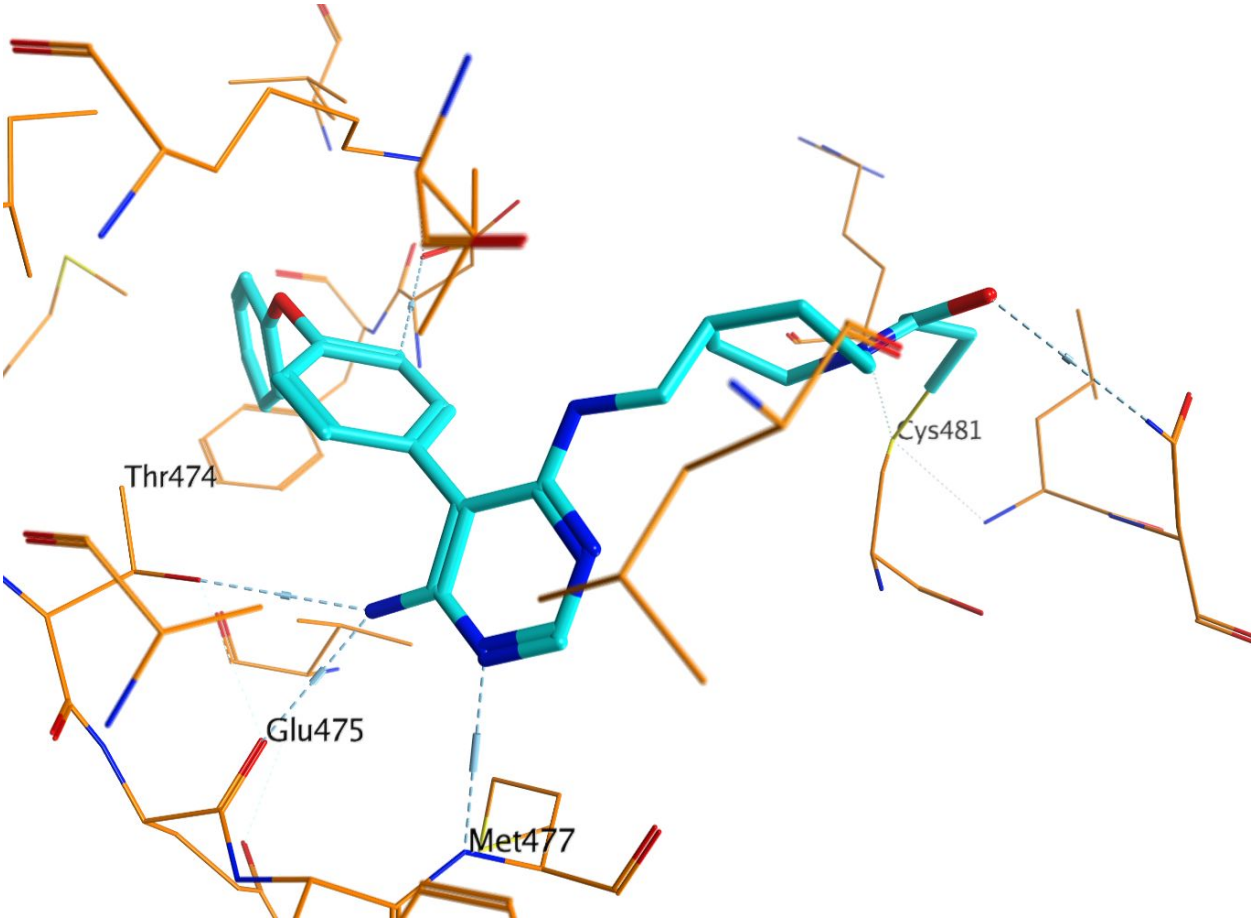

Mass Spectrometry

Reversed-phase (RP)–LC–MS analysis of intact BTK and BTK plus evobrutinib further confirmed the covalent nature of evobrutinib binding and indicated 1:1 stoichiometry (Figure S1 in the Supporting information). Thus, evobrutinib is bound to only one cysteine residue on the BTK kinase domain. Orthogonal confirmation of evobrutinib–BTK covalent binding with 1:1 stoichiometry was also achieved by isothermal calorimetry (see Figure S2 in the Supporting Information).

Jump Dilution Assay

BTK IC_{50} was measured routinely for each compound to drive medicinal chemistry optimization. In addition, a jump dilution assay was used to qualitatively check the irreversible nature of key compounds (see Supporting Information). Lack of recovery of enzymatic activity was consistent with irreversible inhibition of BTK by evobrutinib (Figure S3). In general, time-dependent BTK IC_{50} correlated well with the K_{inact}/K_i ratio (where K_i is the affinity of initial non-covalent binding, and K_{inact} is the maximum potential rate of enzyme inactivation), which represents the second-order rate constant for the reaction of evobrutinib with BTK (Figure S4 and Table S1 in the Supporting Information).[25]

Evobrutinib Kinase Selectivity

The high kinase selectivity of evobrutinib is derived from multiple factors. Its obligate covalent binding to a rare cysteine residue and interaction with a unique threonine gatekeeper-mediated selectivity pocket in structurally related kinases accounts for much of the agent's high kinase selectivity. For kinases with a similarly situated cysteine

residue, selectivity can be explained by examination of the primary structure. The tyrosine kinase BMX, whose sequence identity is the most similar to that of BTK, presented an insurmountable challenge in achieving selectivity (Table S2 in the Supporting information). The Tec kinase ITK also shares a high degree of homology to BTK, but contains a bulky gatekeeper phenylalanine residue, which explains the higher observed selectivity of evobrutinib for BTK over ITK. Conversely, other cysteine containing kinases that are not inhibited by evobrutinib diverge more structurally from BTK, BMX, and ITK (Figure S5 in the Supporting information).

Evobrutinib's selectivity for BTK over EGFR is explained by analysis of the global differences between the structures of the two cysteine-containing kinases. Upon binding to BTK, evobrutinib and ibrutinib resulted in a relatively small displacement of N- and C-lobes in relation to one another. On the other hand, EGFR showed a dramatic rearrangement in the N-lobe when targeted by ibrutinib (Figure S5 in the Supporting Information). It is hypothesized that the 1,3-disubstituted pattern on the piperidine ring in ibrutinib allows the warhead to rotate to adapt to kinases that move their N lobes.[24] In

contrast, the evobrutinib warhead is more constrained having a 1,4-substitution on the piperidine linker and thus cannot accommodate kinases that upon binding rearrange their N lobe, such as EGFR. This is demonstrated in Table 5, which shows that selectivity for BTK over EGFR was lost in **A14** which, similar to ibrutinib, had a 1,3 attachment to the piperidine ring.

Table 5. Selectivity of **A14** and Evobrutinib for BTK and EGFR

Compound	Structure	BTK IC_{50} (nM)	EGFR IC_{50} (nM)
A14	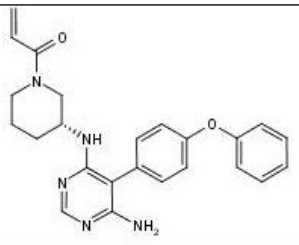	6.5	550
A18 **Evobrutinib**	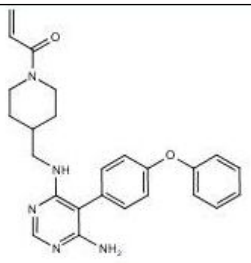	8.9	5800

The higher kinase selectivity of evobrutinib compared with ibrutinib is illustrated in Table 6. Ibrutinib inhibited seven Cys481-containing kinases compared with only two for evobrutinib. Unlike evobrutinib, ibrutinib does not require covalent binding for potency, as it showed only an approximately 10-fold reduction in potency against the Cys481S mutant compared to wildtype BTK. The ibrutinib scaffold, lacking the acrylamide warhead, showed similar potency towards BTK and comparable selectivity against 236 kinases tested.

Table 6. Comparison of Evobrutinib and Ibrutinib Selectivity for BTK and Other Kinases

	Evobrutinib	**Ibrutinib**	**Ibrutinib – no warhead**
BTK IC_{50} (nM)	8.9	0.2	4.5
BTK (Cys481S) KD IC_{50} (nM)	8700	2.2	1.5
Kinase selectivity at 1 μM (number of kinases inhibited by >80% / total number of wildtype kinases tested)	2 / 233	17 / 236	18 / 236

Number of Cys481-containing kinases inhibited	2 (BMX, TEC)	7 (EGFR, ERBB4, BLK, BMX, TEC, TXK, ITK)	4 (BMX, TEC, BLK, TXK)

Preclinical Pharmacokinetic Studies

Evaluation of evobrutinib PK in mice, rats, and dogs indicated that evobrutinib is rapidly absorbed after oral administration, with C_{max} reached between 0.25 and 1 h (Table S3 in the Supporting Information). Evobrutinib demonstrated moderate clearance in mice, and high clearance in rats, and dogs. The plasma half-life was short (~1 h) in all animal species. The oral bioavailability was low (<5% in rats) to moderate (up to 25% in mice) restricted by hepatic and possibly intestinal first-pass metabolism.

Activity of Evobrutinib in Collagen-induced Arthritis

Evobrutinib was tested in a rat collagen-induced arthritis (CIA) model. Female Lewis rats with semi-established type II collagen arthritis[26,27] were treated once daily for 11 days (days 6–16) by oral gavage with vehicle (20% Hydroxy-Propyl-Beta Cyclodextrin in

H_2O), evobrutinib (0.3, 1, 3, 10, or 30 mg/kg), or the reference compound methotrexate (MTX, 0.1 mg/kg). Animals were terminated on study day 17. Efficacy evaluation was based on daily ankle caliper measurements, and histopathologic evaluation of ankles and knees.

Disease-induced ankle-swelling was significantly reduced ($P \leq 0.05$) for rats treated with evobrutinib 3 mg/kg (days 11–17), 10 mg/kg (days 11–17), 30 mg/kg (days 10–17), or MTX (days 11–17), compared with vehicle (Figure 6A). Ankle histopathology scores were also reduced with evobrutinib in a dose-dependent manner, compared to vehicle (Figure 6B). The IC_{50} for evobrutinib was 5.180 mg/kg.

Figure 6. Rat CIA Model: Rats Treated with Evobrutinib, MTX or Vehicle (A) Ankle Thickness, n = 4 for Normal Controls, n = 10 per Treatment Group; $P \leq 0.05$ ANOVA to Vehicle Control; (B) Histopathology Score, n = 10 per Treatment Group; $P \leq 0.05$ ANOVA to Vehicle Control

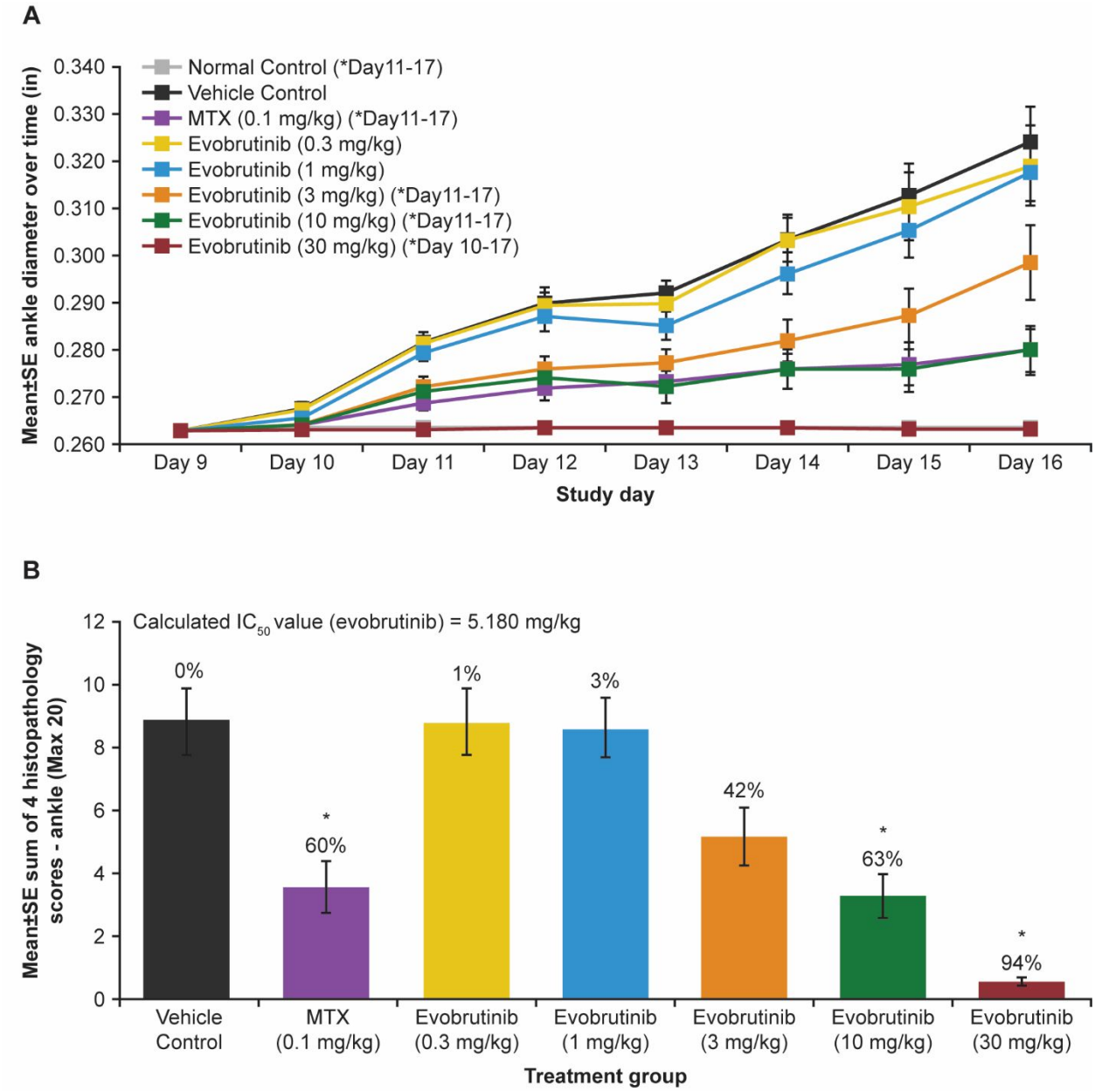

CONCLUSIONS

In summary, we have described the discovery and preclinical characterization of evobrutinib (**A18**), a potent, obligate covalent BTK inhibitor with high kinase selectivity. Evobrutinib was derived from design and subsequent optimization of analogs based on the analysis of the crystal structure of the BTK inhibitor, **B43**. Evobrutinib displayed suitable preclinical pharmacokinetic and promising pharmacodynamic characteristics. Evobrutinib also demonstrated efficacy in a rat model of rheumatoid arthritis.[16] Moreover, the high selectivity of evobrutinib for BTK over EGFR and other Tec family kinases indicates that it may have a low potential for off-target related adverse effects. The results of ongoing clinical trials in various autoimmune diseases will enhance our understanding of the efficacy and safety of evobrutinib.

EXPERIMENTAL SECTION

^{1}H NMR experiments were recorded on a Varian 500 MHz VNMRS Spectrometer equipped with a Varian OneNMR probe, or a Bruker Avance III 400 MHz spectrometer equipped with a Bruker 400 BBO probe. Chemical shifts are expressed in δ ppm referenced to an internal standard, tetramethylsilane (δ = 0 ppm). All microwave reactions were conducted using the Biotage Initiator. All hydrogenation reactions were conducted using the H-Cube apparatus manufactured by ThalesNano. Abbreviations used in describing peak signals are br = broad signal, s = singlet, d = doublet, dd = doublet of doublets, t = triplet, q = quartet, m = multiplet. All final compounds were determined to have purity >95% by HPLC. The purity was assessed using an Agilent 1100 HPLC system (Agilent Technologies) with an XBridge column (C18, 3.5 μm, 4.6 x 50 mm). Mass spectra were recorded on an electrospray mass spectrometer (ES-MS) in electrospray ionization positive (ESI+) mode. High-resolution mass spectrometry (HRMS) experiments were performed on a CapLC (1100 series, Agilent Technologies) which was coupled to the Synapt G1 HDMS (Waters, Milford, MA) mass spectrometer using ESI as the ionization source.

Synthesis of A3, A8, A9, A18 (synthesis of A4–A7, A10-A17, A19-A31 is shown in the Supporting Information) ***N*-(3-{[6-amino-5-(4-phenoxyphenyl)pyrimidin-4-yl]oxy}phenyl)acrylamide (A3)** Step 1: To a 20-mL microwave vial with stir bar, was added 5,6-dichloropyrimidin-4-amine (300.00 mg, 1.83 mmol), 3-aminophenol (0.30 g, 2.74 mmol; 1.50 eq.) and cesium carbonate (894.06 mg, 2.74 mmol) followed by *N*, *N*-dimethyl-acetamide (4.00 mL). The reaction mixture was run in a microwave at 150 °C for 1 h before it was filtered. The collected solution (6-(3-aminophenoxy)-5-chloropyrimidin-4-amine) was concentrated and carried to the next step without further purification. [ES-MS] (ESI+): *m*/*z* calcd for $C_{10}H_{10}ClN_4O$ $[M + H]^+$, 237; found, 237.

Step 2: To a microwave vial containing 6-(3-amino-phenoxy)-5-chloro-pyrimidin-4-ylamine (433.08 mg, 1.83 mmol), (4-phenoxyphenyl)boronic acid (450.42 mg, 2.10 mmol) and cesium carbonate (1311.78 mg, 4.03 mmol), was added dioxane (14 mL) and water (1.4 mL). The mixture was degassed for 5 min with N_2 before palladium(ii) acetate (20.54 mg, 0.09 mmol) and 2-dicyclohexylphosphino-2',6'-dimethoxybiphenyl (75.13 mg, 0.18 mmol) were added. The reaction was microwaved at 150 °C for 90 min before it was filtered through a filtration funnel with a Celite pad. The collected solution was concentrated and purified by silica gel chromatography (28 g silica, ethyl acetate/methanol = 1/10) to give 6-(3-Amino-phenoxy)-5-(4-phenoxy-phenyl)-pyrimidin-4-ylamine (1.17g, 70% yield) as a yellow solid. [ES-MS] (ESI+): *m*/*z* calcd for $C_{22}H_{19}N_2O_4$ $[M + H]^+$, 371; found, 371.

Step 3: To a 20-mL reaction vial, was added acrylic acid (0.01 mL, 0.12 mmol), bis(2-oxo-3-oxazolidinyl)phosphinic chloride (42.04 mg, 0.17 mmol), dioxane (3.00 mL) and *N*,*N*-diisopropylethylamine (0.07 mL, 0.41 mmol). The mixture was stirred at room temperature for 1

h before 6-(3-aminophenoxy)-5-(4-phenoxyphenyl) pyrimidin-4-amine (40.00 mg, 0.08 mmol) was added. The reaction was stirred at room temperature overnight. The reaction was stirred at room temperature for 12 h before it was concentrated and purified by silica gel chromatography (25g Biotage silicon column, 50–100% ethyl acetate/hexane, then 0–40 % methanol/ethyl acetate) to afford the title compound (**A3**) (7 mg, 20% yield) as a white solid. ^{1}H-NMR (DMSO-d_6) δ 10.14 (s, 1 H), 8.00 (s, 1 H), 7.41 (s, 1 H), 7.36-7.30 (m, 5H), 7.22 (t, 1 H), 7.09 (t, 1 H), 7.03–7.01 (m, 4H), 6.71 (d, 1 H), 6.53 (broad s, 2H), 6.34 (dd, 1 H), 6.1 8 (d, 1 H), 5.69 (d, 1 H). [ES-MS] (ESI+): *m*/*z* calcd for $C_{25}H_{21}N_4O_3$ $[M + H]^+$, 425; found, 425.

***N*-{3-[6-Amino-5-(4-phenoxy-phenyl)-pyrimidin-4-ylamino]-phenyl}-acrylamide (A8)** Step 1: Into a 20-mL vial was placed 5,6-dichloropyrimidin-4-amine (500 mg, 3.05 mmol) was added benzene-1 ,3-diamine (329.72 mg, 3.05 mmol) and a pre-made mixture of TFA:TEA (1:1 mol) (347.64 mg: 308.52 mg) dissolved in DMSO (6 mL). The mixture was heated at 90°C overnight before it was purified by silica gel chromatography (25 g Biotage silicon column, 0–40% methanol/ethyl acetate) to afford *N*-4-(3-aminophenyl)-5-chloropyrimidine-4,6-diamine (591 mg, 82% yield) as a brown syrup. [ES-MS] (ESI+): *m*/*z* calcd for $C_{10}H_{11}ClN_5$ $[M + H]^+$, 236; found, 236.

Step 2: Into a 20-mL microwave vial was placed *N*-(3-amino-phenyl)-5-chloro-pyrimidine-4,6-diamine (200.00 mg, 0.85 mmol), (4-phenoxyphenyl)boronic acid (272.45 mg, 1.27 mmol), palladium acetate (9.53 mg; 0.04 mmol; 0.05 eq.), 2-dicyclohexylphosphino-2',6'-dimethoxybiphenyl (34.84 mg, 0.08 mmol), and potassium carbonate (351.86 mg, 2.55 mmol) followed by dissolved dioxane (3.00 mL) and water (0.30 mL). The reaction was stirred at 150 ^{o}C for 3 h before it was concentrated and purified by silica gel chromatography (25 g, 80–100% EtOAc/Hexanes, then 0–20% methanol/ethyl acetate) to afford the *N*-4-(3-aminophenyl)-5-(4-

phenoxyphenyl)pyrimidine-4,6-diamine (167.90 mg, 54% yield) as a yellow solid. [ES-MS] (ESI+): *m*/*z* calcd for $C_{22}H_{20}N_5O$ $[M + H]^+$, 370; found, 370.

Step 3: In a vial was placed N-(3-amino-phenyl)-5-(4-phenoxy-phenyl)-pyrimidine-4,6-diamine (400.00 mg, 1.08 mmol) in DCM (10.00 mL, 156.01 mmol), ethyl-diisopropyl-amine (0.72 mL; 4.33 mmol; 4.00 eq.), acrylic acid (156.06 mg, 2.17 mmol) and 2,4,6-tripropyl-1,3,5,2,4,6-trioxatriphosphinane 2,4,6-trioxide (1.28 mL, 4.33 mmol). The reaction was stirred at room temperature for 2 h before it was purified with prep-HPLC (38–42% acetonitrile in 0.1% NH_4OH in H_2O) to afford the title compound (**A8**) (166 mg, 36% yield) as a white solid. ^{1}H-NMR (DMSO-d_6) δ 10.03 (s, 1 H), 8.08 (s, 1H), 7.73 (s, 1H), 7.32 (m, 2H), 7.27 (m, 3H), 7.17 (m, 8H), 6.45 (m, 1H), 6.25 (m, 1H), 5.73 (m, 3H). [ES-MS] (ESI+): *m*/*z* calcd for $C_{25}H_{22}N_5O$ $[M + H]^+$, 424; found, 424.

***N*-(*cis*-(3-{[6-amino-5-(4-phenoxyphenyl)pyrimidin-4-yl]amino}cyclohexyl)prop-2-enamide (A9)** Step 1: Into a 20-mL vial was placed 5,6-dichloro-pyrimidin-4-ylamine (600.00 mg, 3.66 mmol), *cis*-tert-butyl N-(3-aminocyclohexyl)carbamate (940.89 mg, 2.20 mmol) and ethyl-diisopropyl-amine (1.91 mL; 10.98 mmol; 3.00 eq.) followed by NMP (6.00 mL). The reaction was stirred at 160 °C for 3 h before it was purified by silica gel chromatography (50 g, 30–80% ethyl acetate/hexanes) to afford *cis*-tert-butyl N-{3-[(6-amino-5-chloropyrimidin-4-yl)amino]cyclohexyl}carbamate (429.90 mg, 17.2% yield) as a yellow solid. [ES-MS] (ESI+): *m*/*z* calcd for $C_{15}H_{25}ClN_5O_2$ $[M + H]^+$, 342; found, 342

Step 2: Into a 20-mL microwave vial was placed *cis*-tert-butyl N-{3-[(6-amino-5-chloropyrimidin-4-yl)amino]cyclohexyl}carbamate (420.00 mg; 0.61 mmol; 1.00 eq.), 4-phenoxyphenyl)boronic acid (394.45 mg, 1.84 mmol), palladium acetate (13.79 mg, 0.06

mmol), 2-dicyclohexylphosphino-2',6'-dimethoxybiphenyl (50.44 mg, 0.12 mmol), potassium carbonate (509.42 mg, 3.69 mmol) followed by dioxane (4.00 mL) and water (0.40 mL). The reaction was heated for 3 h at 150 °C before it was purified by silica gel chromatography (25 g, 60–100% ethyl acetate/hexane, then 0-20% MeOH/EtOAc) to afford *cis*-tert-butyl N-(3-{[6-amino-5-(4-phenoxyphenyl)pyrimidin-4-yl]amino}cyclohexyl)carbamate (399.00 mg, 68% yield) as a white solid. [ES-MS] (ESI+): *m/z* calcd for $C_{27}H_{34}N_5O_3$ $[M + H]^+$, 476; found, 476.

Step 3: Into a 20-mL vial containing *cis*-tert-butyl N-(3-{[6-amino-5-(4-phenoxyphenyl)pyrimidin-4-yl]amino}cyclohexyl)carbamate (700.00 mg, 0.74 mmol), methanol (5.00 mL) was added hydrogen chloride (3.68 mL, 7.36 mmol) (2.0 M solution in Et_2O). The reaction was stirred at room temperature for 12 h before it was concentrated and *cis*-N4-(3-aminocyclohexyl)-5-(4-phenoxyphenyl)pyrimidine-4,6-diamine was used in the next step without further purification. [ES-MS] (ESI+): *m/z* calcd for $C_{22}H_{26}N_5O$ $[M + H]^+$, 376; found, 376.

Step 4: To a 20-mL vial was added *cis*-N4-(3-aminocyclohexyl)-5-(4-phenoxyphenyl)pyrimidine-4,6-diamine (550.00 mg, 0.73 mmol), sodium hydrogen carbonate (369.17 mg, 4.39 mmol) suspended in water (2.00 mL) and THF (20.00 mL) and acryloyl chloride (0.15 mL, 1.83 mmol). The reaction was stirred at room temperature for 12 h before it was purified by silica gel chromatography (55 g KPNH Silica, 0–100% methanol/ethyl acetate) to afford the title compound (**A9**) (40 mg, 13% yield) as a white solid. ^{1}H-NMR (DMSO-d_6) δ 7.94 (m, 2H), 7.41 (m, 2H), 7.12 (m, 7H), 6.06 (m, 2H), 5.5 (m, 3H), 4.80 (d, J = 8 Hz, 1H), 3.92 (m, 1H), 3.61 (m, 1H), 1.95 (m, 1H), 1.70 (m, 3H), 1.25 (m, 1H), 1.07 (m, 3H). [ES-MS] (ESI+): *m/z* calcd for $C_{25}H_{28}N_5O_2$ $[M + H]^+$, 430; found, 430.

***N*-[(1-acryloylpiperidin-4-yl)methyl]-5-(4-phenoxyphenyl)pyrimidine-4,6-diamine**

(A18) Step 1: A suspension of 5,6-dichloro-pyrimidin-4-ylamine (1.00 g, 6.10 mmol) in dry *N*, *N*-dimethylformamide (10 mL) was treated with 4-aminomethyl-piperidine-1-carboxylic acid tert-butyl ester (1.62 mL, 7.62 mmol) followed by DBU (1.19 mL, 7.93 mmol). The contents were heated to 90 °C for 17 h (overnight). Water (2 mL) was then added to the reaction and the resulting white suspension was stirred overnight. The solids were filtered and dried under high vacuum to give *tert*-butyl 4-{[(6-amino-5-chloropyrimidin-4-yl)amino]methyl}piperidine-1-carboxylate (1.90 g, 91.2%) as a white solid. ^{1}H-NMR (DMSO-d_6) δ 7.81 (s, 1H), 6.66 (t, J= 4Hz, 1H), 6.42 (s, 2H), 3.89 (d, J = 16 Hz, 2H), 3.23 (m, 2H), 2.66 (d, J = 4Hz, 1H), 1.75 (m, 1H), 1.59 (d, J = 12 Hz, 2H), 1.39 (s, 9H), 1.0 (m, 2H). [ES-MS] (ESI+): *m*/*z* calcd for $C_{15}H_{25}ClN_5O_2$ $[M + H]^+$, 342; found, 342.

Step 2: Into a 20-mL microwave vial was placed tert-butyl 4-[(6-amino-5-chloropyrimidin-4-yl)amino]methylpiperidine-1-carboxylate (797.30 mg; 2.33 mmol), (4-phenoxyphenyl)boronic acid (748.79 mg; 3.50 mmol), palladium(ii) acetate (26.18 mg; 0.12 mmol), 2-dicyclohexylphosphino-2',6'-dimethoxybiphenyl (95.75 mg; 0.23 mmol), potassium carbonate (967.03 mg; 7.00 mmol), dioxane (9.00 mL) and water (0.90 mL). The reaction was then heated in the microwave for 2 h at 150 °C. The reaction mixture was then filtered, then concentrated to dryness. The resulting residue was dissolved with DCM (2mL) then purified by silica gel chromatography (50 g, 80-100% EtOAc/Hexanes, then 0-40% MeOH/EtOAc) to give *tert*-butyl 4-({[6-amino-5-(4-phenoxyphenyl)pyrimidin-4-yl]amino}methyl)piperidine-1-carboxylate (534.6 mg, 48.2% yield). [ES-MS] (ESI+): *m*/*z* calcd for $C_{27}H_{34}N_5O_3$ $[M + H]^+$, 476; found, 476.

Step 3: Into a 20-mL vial containing 4-([6-amino-5-(4-phenoxyphenyl)pyrimidin-4-yl]aminomethyl)piperidine-1-carboxylate (534.60 mg; 1.12 mmol; 1.00 eq.) methanol (4.00 mL) was added hydrogen chloride (5.62 mL, 11.24 mmol) (2.0 M solution in Et_2O). The reaction was stirred at room temperature for 18 h. The reaction was then concentrated to dryness to give 5-(4-phenoxyphenyl)-N-(piperidin-4-ylmethyl)pyrimidine-4,6-diamine which was used without purification. [ES-MS] (ESI+): *m/z* calcd for $C_{22}H_{26}N_5O$ $[M + H]^+$, 376; found, 376.

Step 4: To a 20-mL vial was added 5-(4-phenoxyphenyl)-N-(piperidin-4-ylmethyl)pyrimidine-4,6-diamine (210.00 mg; 0.56 mmol; 1.00 eq.), sodium bicarbonate (70.48 mg; 0.84 mmol; 1.50 eq.), THF (8.00 mL; 98.74 mmol; 176.55 eq.) and water (0.80 mL; 44.41 mmol; 79.40 eq.). The mixture was cooled to 0 °C on an ice bath. Acryloyl chloride (0.15 mL, 1.83 mmol) was then added dropwise. The ice bath was removed and the reaction was stirred at room temperature for 12 h before it was purified by silica gel chromatography (25 g KPNH Silica, 0–100% methanol/ethyl acetate) to afford the title compound (**A18**) (21 mg, 8.7% yield) was synthesized with a similar protocol to prepared as described in the main body of the article. ^{1}H-NMR (DMSO-d_6) δ 7.93 (s, 1 H), 7.40 -7.08 (m, 9H), 6.76 (dd, J = 4 Hz, 1 H), 6.04 (d, J = 4 Hz, 1 H), 5.61 (d, J = 4 Hz, 1 H), 5.43 (s, 2H), 4.34 (d, J = 12 Hz, 1 H), 3.98 (d, J = 8 Hz, 1 H), 3.12 (m, 2H), 2.95 (m, 1 H), 2.56 (m, 1 H), 1.81 (m, 1 H), 1.59 (m, 2H), 0.92 (m, 2H). [ES-MS] (ESI+): *m/z* calcd for $C_{25}H_{28}N_5O_2$ $[M + H]^+$, 430; found, 430.

ASSOCIATED CONTENT

Supporting Information.

S3–S6 Assay Details

S6–S7 Mass Spectrometry

S8–S9 Isothermal Calorimetry

S10–S15 Jump Dilution Assay

S16–S20 Kinase Selectivity

S20 Animal Studies

S21–S22 Preclinical PK Studies

S23–S38 Synthesis of Compounds **A4–A7, A10–A17, A19**

S38–S46 Synthesis of Compounds **A20–A26**

S47–S51 Synthesis of Compounds **A27–A31**

S51–S52 References

Molecular Formula Strings and some data

PDB ID CODES [3gen; 5p9j;5yu9]. Authors will release the atomic coordinates and experimental data upon article publication.

AUTHOR INFORMATION

Corresponding Author

*Richard D. Caldwell

EMD Serono Research & Development Institute, Inc. (a business of Merck KGaA,

Darmstadt, Germany),

45 A Middlesex Turnpike, Billerica, MA 01821, USA

Tel: 978 -294-1100

Fax: 781-681-2691

Email: richard.caldwell@emdserono.com.

*Hui Qiu

EMD Serono Research & Development Institute, Inc. (a business of Merck KGaA,

Darmstadt, Germany),

45 A Middlesex Turnpike, Billerica, MA 01821, USA

Tel: +1 978 294 1442

Fax: +1 978 294 1400

E-mail: hui.qiu@emdserono.com

Present author addresses

†Author present address

B.C.A.: Breakthrough Chemistry Advisors, 266 Arrowhead Road, Marshfield, MA 02050, USA

‡Author present address

M.C.: 45 Chemin de Cazers Bas 81100 Castres France (no current affiliation)

§Author present address

A.S.G.: Constellation Pharmaceuticals, 215 First Street, Suite 200, Cambridge, MA 02142, USA

‖Author present address

B.H.: UMass Boston - Venture Development Center, 100 Morrissey Boulevard, Boston, MA 02125, USA

¶Author present address

B.L.H.: Accent Therapeutics, 65 Hayden Avenue, Lexington, Cambridge, MA 02421, USA

††Author present address

I.M.: Vertex Pharmaceuticals, 3215 Merryfield Row, San Diego, CA 92121

‡‡Author present address

F.M.: Roche Innovation Centre Basel, Pharma Research and Early Development, Hoffmann La Roche, Basel, Switzerland.

§§Author present address

N.N.: Advanced Instruments, LLC., Two Technology Way, Norwood, MA 02062, USA

¶¶Author present address

M.M.: Nuvisan GmbH, Site Grafing, Am Feld 32, 85567 Grafing, Germany

‖‖Author present address

A.S.: Boston Cheese Cellar, 8 Birch St, Roslindale, MA 02131, USA

Author Contributions

The manuscript was written through contributions of all authors. All authors have given approval to the final version of the manuscript.

Funding Sources

This work was funded by EMD Serono Inc. (a business of Merck KGaA, Darmstadt, Germany).

Notes

The authors declare the following competing financial interest(s):

All authors are or were employees of EMD Serono (a business of Merck KGaA, Darmstadt, Germany) at the time that the work was conducted.

ACKNOWLEDGMENT

The authors would like to thank Dr Momar Toure and Dr Shashank Kulkarni from EMD Serono for their guidance in drafting and reviewing the manuscript. Medical writing support was provided by Fiona Scott, PhD, Bioscript Science, Macclesfield, UK, and funded by Merck KGaA, Darmstadt, Germany. The manuscript was written in accordance with Good Publication Practice (GPP3) guidelines (http://www.ismpp.org/gpp3).

ABBREVIATIONS USED:

BCR, B cell receptor; BTK, Bruton's tyrosine kinase; Cl_{int}, intrinsic clearance; CLL, chronic lymphocytic leukemia; C_{max}, maximum plasma concentration; EGFR, epidermal growth factor receptor; ES-MS, electrospray-mass spectrometer; FcγR, Fc-gamma receptor; FDA, Food and Drug Administration; hERG, human ether-a-go-go-related gene; HLM, human liver microsomes; HRMS, high-resolution-mass spectrometer; IC_{50}, half maximal inhibitory concentration; Ki, inhibitory constant; MCL, mantle cell lymphoma; PBMC,

peripheral blood mononuclear cell; PD, pharmacodynamic; PK, pharmacokinetic; SAR, structure–activity relationship

REFERENCES

(1) Brunner, C.; Muller, B.; Wirth, T. Bruton's tyrosine kinase is involved in innate and adaptive immunity. *Histol. Histopathol.* **2005,** 20, 945-955.

(2) Satterthwaite, A. B.; Li, Z.; Witte, O. N. Btk function in B cell development and response. *Semin. Immunol.* **1998,** 10, 309-316.

(3) Yu, P. W.; Tabuchi, R. S.; Kato, R. M.; Astrakhan, A.; Humblet-Baron, S.; Kipp, K.; Chae, K.; Ellmeier, W.; Witte, O. N.; Rawlings, D. J. Sustained correction of B-cell development and function in a murine model of X-linked agammaglobulinemia (XLA) using retroviral-mediated gene transfer. *Blood* **2004,** 104, 1281-1290.

(4) Khan, W. N. Regulation of B lymphocyte development and activation by Bruton's tyrosine kinase. *Immunol. Res.* **2001,** 23, 147-156.

(5) Nyhoff, L. E.; Clark, E. S.; Barron, B. L.; Bonami, R. H.; Khan, W. N.; Kendall, P. L. Bruton's tyrosine kinase is not essential for B cell survival beyond early developmental stages. *J. Immunol.* **2018,** 200, 2352-2361.

(6) Di Paolo, J. A.; Huang, T.; Balazs, M.; Barbosa, J.; Barck, K. H.; Bravo, B. J.; Carano, R. A.; Darrow, J.; Davies, D. R.; DeForge, L. E.; Diehl, L.; Ferrando, R.; Gallion, S. L.; Giannetti, A. M.; Gribling, P.; Hurez, V.; Hymowitz, S. G.; Jones, R.; Kropf, J. E.; Lee, W. P.; Maciejewski, P. M.; Mitchell, S. A.; Rong, H.; Staker, B. L.; Whitney, J. A.; Yeh, S.; Young, W. B.; Yu, C.; Zhang, J.; Reif, K.; Currie, K. S. Specific Btk inhibition suppresses B cell- and myeloid cell-mediated arthritis. *Nat. Chem. Biol.* **2011,** 7, 41-50.

(7) Puri, K. D.; Di Paolo, J. A.; Gold, M. R. B-cell receptor signaling inhibitors for treatment of autoimmune inflammatory diseases and B-cell malignancies. *Int. Rev. Immunol.* **2013,** 32, 397-427.

(8) Byrd, J. C.; Brown, J. R.; O'Brien, S.; Barrientos, J. C.; Kay, N. E.; Reddy, N. M.; Coutre, S.; Tam, C. S.; Mulligan, S. P.; Jaeger, U.; Devereux, S.; Barr, P. M.; Furman, R. R.; Kipps, T. J.; Cymbalista, F.; Pocock, C.; Thornton, P.; Caligaris-Cappio, F.; Robak, T.; Delgado, J.; Schuster, S. J.; Montillo, M.; Schuh, A.; de Vos, S.; Gill, D.; Bloor, A.; Dearden, C.; Moreno, C.; Jones, J. J.; Chu, A. D.; Fardis, M.; McGreivy, J.; Clow, F.; James, D. F.; Hillmen, P.; Resonate Investigators. Ibrutinib versus ofatumumab in previously treated chronic lymphoid leukemia. *N. Engl. J. Med.* **2014,** 371, 213-223.

(9) Byrd, J. C.; Harrington, B.; O'Brien, S.; Jones, J. A.; Schuh, A.; Devereux, S.; Chaves, J.; Wierda, W. G.; Awan, F. T.; Brown, J. R.; Hillmen, P.; Stephens, D. M.; Ghia, P.; Barrientos, J. C.; Pagel, J. M.; Woyach, J.; Johnson, D.; Huang, J.; Wang, X.; Kaptein, A.; Lannutti, B. J.; Covey, T.; Fardis, M.; McGreivy, J.; Hamdy, A.; Rothbaum, W.; Izumi, R.; Diacovo, T. G.; Johnson, A. J.; Furman, R. R. Acalabrutinib (ACP-196) in relapsed chronic lymphocytic leukemia. *N. Engl. J. Med.* **2016,** 374, 323-332.

(10) Bitar, C.; Sadeghian, A.; Sullivan, L.; Murina, A. Ibrutinib-associated pityriasis rosea-like rash. *JAAD Case Rep.* **2018,** 4, 55-57.

(11) de Weerdt, I.; Koopmans, S. M.; Kater, A. P.; van Gelder, M. Incidence and management of toxicity associated with ibrutinib and idelalisib: a practical approach. *Haematologica* **2017,** 102, 1629-1639.

(12) McMullen, J. R.; Boey, E. J.; Ooi, J. Y.; Seymour, J. F.; Keating, M. J.; Tam, C. S. Ibrutinib increases the risk of atrial fibrillation, potentially through inhibition of cardiac PI3K-Akt signaling. *Blood* **2014,** 124, 3829-3830.

(13) Wu, J.; Liu, C.; Tsui, S. T.; Liu, D. Second-generation inhibitors of Bruton tyrosine kinase. *J. Hematol. Oncol.* **2016,** 9, 80.

(14) US Food and Drug Administration. CALQUENCE® (acalabrutinib) US Prescribing Information https://www.accessdata.fda.gov/drugsatfda_docs/label/2017/210259s000lbl.pdf (accessed December 6, 2018).

(15) Haselmayer, P.; Camps, M.; Liu-Bujalski, L.; Nguyen, N.; Morandi, F.; Head, J.; O'Mahony, A.; Zimmerli, S. C.; Bruns, L.; Bender, A.; Schroeder, P.; Grenningloh, R. Efficacy and pharmacodynamic modeling of the BTK inhibitor evobrutinib in autoimmune disease models. *J. Immunol.* **2019,** 202, 2888-2906.

(16) Montalban, X.; Arnold, D. L.; Weber, M. S.; Staikov, I.; Piasecka-Stryczynska, K.; Willmer, J.; Martin, E. C.; Dangond, F.; Syed, S.; Wolinsky, J.; on behalf of the Evobrutinib Phase 2 Study Group. Placebo-controlled trial of an oral BTK inhibitor in multiple sclerosis. *N. Engl. J. Med.* **2019,** 380, 2406-2417.

(17) Ulrich, R. G. Idiosyncratic toxicity: a convergence of risk factors. *Annu. Rev. Med.* **2007,** 58, 17-34.

(18) Lou, Y.; Owens, T. D.; Kuglstatter, A.; Kondru, R. K.; Goldstein, D. M. Bruton's tyrosine kinase inhibitors: approaches to potent and selective inhibition, preclinical and clinical evaluation for inflammatory diseases and B cell malignancies. *J. Med. Chem.* **2012,** 55, 4539-4550.

(19) Pan, Z.; Scheerens, H.; Li, S. J.; Schultz, B. E.; Sprengeler, P. A.; Burrill, L. C.; Mendonca, R. V.; Sweeney, M. D.; Scott, K. C.; Grothaus, P. G.; Jeffery, D. A.; Spoerke, J. M.; Honigberg, L. A.; Young, P. R.; Dalrymple, S. A.; Palmer, J. T. Discovery of selective irreversible inhibitors for Bruton's tyrosine kinase. *ChemMedChem.* **2007,** 2, 58-61.

(20) Marcotte, D. J.; Liu, Y. T.; Arduini, R. M.; Hession, C. A.; Miatkowski, K.; Wildes, C. P.; Cullen, P. F.; Hong, V.; Hopkins, B. T.; Mertsching, E.; Jenkins, T. J.; Romanowski, M. J.; Baker, D. P.; Silvian, L. F. Structures of human Bruton's tyrosine kinase in active and inactive conformations suggest a mechanism of activation for TEC family kinases. *Protein Sci.* **2010,** 19, 429-439.

(21) Qiu, H.; Liu-Bujalski, L.; Caldwell, R. D.; Follis, A. V.; Gardberg, A.; Goutopoulos, A.; Grenningloh, R.; Head, J.; Johnson, T.; Jones, R.; Mochalkin, I.; Morandi, F.; Neagu, C.; Sherer, B. Discovery of potent, highly selective covalent irreversible BTK inhibitors from a fragment hit. *Bioorg. Med. Chem. Lett.* **2018,** 28, 2939-2944.

(22) Jackson, P. A.; Widen, J. C.; Harki, D. A.; Brummond, K. M. Covalent modifiers: a chemical perspective on the reactivity of alpha,beta-unsaturated carbonyls with thiols via hetero-Michael addition reactions. *J. Med. Chem.* **2017,** 60, 839-885.

(23) Schwobel, J. A.; Wondrousch, D.; Koleva, Y. K.; Madden, J. C.; Cronin, M. T.; Schuurmann, G. Prediction of Michael-type acceptor reactivity toward glutathione. *Chem. Res. Toxicol.* **2010,** 23, 1576-1585.

(24) Bender, A. T.; Gardberg, A.; Pereira, A.; Johnson, T.; Wu, Y.; Grenningloh, R.; Head, J.; Morandi, F.; Haselmayer, P.; Liu-Bujalski, L. Ability of Bruton's tyrosine kinase inhibitors to sequester Y551 and prevent phosphorylation determines potency for inhibition of Fc receptor but not B-cell receptor signaling. *Mol. Pharmacol.* **2017,** 91, 208-219.

(25) Singh, J.; Petter, R. C.; Baillie, T. A.; Whitty, A. The resurgence of covalent drugs. *Nat. Rev. Drug Discov.* **2011,** 10, 307-317.

(26) Bendele, A. Animal models of rheumatoid arthritis. *J. Musculoskelet. Neuron. Interact.* **2001,** 1, 377-385.

(27) Bolder BioPath. Collagen Induced Arthritis (CIA) in Rat. https://bolderbiopath.com/study/collagen-induced-arthritis-rat/ (accessed January 7, 2018).

TABLE OF CONTENTS GRAPHIC